Application of Site-directed Metal Chelation Techniques to Structure Determination of *Pyrococcus furiosus* RNase P

Honors Research Thesis

Presented in partial fulfillment of the requirements for graduation *with honors research distinction* in Biochemistry in the undergraduate colleges of The Ohio State University

by

Ian L. T. Smith

The Ohio State University
June 2011

Project Advisor: Professor Mark P. Foster, Department of Biochemistry

This document is dedicated to Ribonuclease P.

TABLE OF CONTENTS

LIST OF ABBREVIATIONS

cDNA	complementary DNA
CVs	column volumes
D_2O	deuterium oxide
ddNTP	dideoxynucleoside triphosphate
DNA	deoxyribonucleic acid
DSS	4,4-dimethyl-4-silapentane-1-sulfonic acid
DTNB	Ellman's reagent: 5,5'-dithio-bis-(2-nitrobenzoic acid)
DTT	dithiothreitol
E. coli	*Escherichia coli*
EDTA	ethylenediaminetetraacetic acid
EPD	EDTA-2-aminoethyl 2-pyridyl disulfide
ESI	electrospray ionization
Fe^{3+}	iron (III)
FPLC	fast protein liquid chromatography
HSQC	heteronuclear single-quantum coherence
IPTG	isopropyl β-D-1-thiogalactopyranoside
LB	lysogeny broth
m/z	mass to charge ratio
MALDI	matrix assisted laser desorption/ionization
Mja	*Methanocaldoccus jannaschii*
Mn^{2+}	manganese (II)
NMR	nuclear magnetic resonance
NOESY	nuclear Overhauser effect spectroscopy
NTP	nucleoside triphosphate
PAGE	polyacrylamide gel electrophoresis
Pfu	*Pyrococcus furiosus*
Pho	*Pyrococcus horikoshii*
PMSF	phenylmethanesulfonylfluoride
PRE	paramagnetic relaxation enhancement
ptRNA	precursor tRNA
RNA	ribonucleic acid
RNase	ribonuclease
RPM	rotations per minute
RPP	RNase P protein
RPR	RNase P RNA
TNB	2-nitro-5-thiobenzoic acid
tRNA	transfer ribonucleic acid

LIST OF FIGURES

LIST OF TABLES

ABSTRACT

Ribonuclease (RNase) P is a ribonucleoprotein complex that is responsible for cleaving the 5' leader sequence during the maturation of tRNA molecules. Its three-dimensional structure yet unknown, RNase P in human nuclei is thought to contain ten protein subunits and one RNA subunit. In contrast, RNase P in the hyperthermophilic archaeon *Pyrococcus furiosus* (*Pfu*) is simpler, with only five protein subunits and one RNA subunit. Though the three-dimensional structure of the archaeal holoenzyme is also unknown, all five protein subunits are homologous to corresponding subunits in human RNase P. Due to its more tractable configuration, yet maintained homology, analysis of *Pfu* RNase P is attractive as a model to provide insights into the structure and function of the human enzyme. The long-term goal of this project is to develop an atomic-resolution model of the *Pfu* RNase P holoenzyme. To aid in structure determination of this ribonucleoprotein complex, the attachment of an ethylenediaminetetraacetic acid (EDTA) moiety to strategically-located cysteine residues on one of the protein subunits was explored in order to exploit the EDTA moiety's metal-chelating capabilities in two distinct ways. The chelation of paramagnetic Mn^{2+} allowed for the execution of paramagnetic relaxation enhancement (PRE) nuclear magnetic resonance (NMR) experiments. This unconventional NMR method enables distance restraints to be obtained over larger distances than conventional NMR methods. The chelation of iron atoms allowed for the implementation of RNA footprinting experiments by utilizing Fe·EDTA-generated hydroxyl radicals: the hydroxyl radicals cleave nucleic acid in a distance-dependent manner. Thus, preparation of chelator-tagged proteins was shown to provide valuable information to constrain structural models of the *Pfu* RNase P holoenzyme.

INTRODUCTION

RNase P

Ribonuclease (RNase) P is an endoribonuclease that is responsible for catalyzing the essential cleavage reaction to remove the 5'-leader sequence from precursor transfer ribonucleic acid (ptRNA) molecules [1-3]. Discovered by Dr. Sidney Altman in 1970, RNase P is found in all three phylogenetic domains of life: bacteria, archaea, and eukarya [2, 4]. Altman later determined that RNase P from *Escherichia coli* (*E. coli*) contains a catalytic RNA core, for which he was subsequently awarded the 1989 Nobel Prize in Chemistry, along with Dr. Thomas Cech, for this discovery that RNA can act as a biocatalyst [5]. RNase P is essentially required for life; there are only a few known organisms that lack RNase P [6]. Moreover, RNase P exists almost universally as a ribonucleoprotein; one noteworthy exception is human mitochondrial RNase P, which functions as a protein enzyme [7]. In addition to processing ptRNAs, RNase P has also been shown to cleave messenger RNA transcripts, polycistronic tRNA, precursor 4.5S RNA, precursor tmRNA, and certain riboswitches [8-11].

Despite its prevalence across the three domains of life, this ribozyme exhibits varied structural composition. In general, more complex organisms contain a greater number of RNase P proteins (RPPs) than do simpler organisms: in bacteria, RNase P exists as the RNase P RNA (RPR) subunit in complex with one RPP. In archaea, the RPR is joined by at least four RPPs, and eukaryotes have the RPR and at least nine RPPs [12]. This pattern of increasing protein content in more evolutionarily complex organisms suggests that RNase P is perhaps a partial holdover from the RNA world [13].

The Rationale for Studying RNase P from *Pyrococcus furiosus*

While certain functions of RNase P have already been illuminated, the overall structure of the ribonucleoprotein complex in higher organisms has yet to be determined. Given the essential role of RNase P in processing ptRNA, structural differences between the human version and RNase P in pathogenic organisms could provide an attractive avenue for antimicrobial chemotheraphy [14]. Therefore, solving RNase P structures could provide useful insights for such drug development, as well as elucidate how the ribozyme functions at an atomic level. The hyperthermophilic archaeon *Pyrococcus furiosus* (*Pfu*), an anaerobic heterotroph that was originally isolated from geothermal vents in Italy, provides a tractable system that also maintains homology with the human enzyme [15]. Though the bacterial ribonucleoprotein complex is simplest in composition, with only one RPP joining the RNA subunit, none of the archaeal or eukaryal RPPs possesses appreciable sequence homology to the bacterial RPP. *Pfu* RNase P, in contrast, is composed of five RPPs that are all homologous to RPPs in human nuclear RNase P, and reconstitution of eukaryal RNase P remains challenging [16, 17].

The five RPPs in *Pfu* are homologs of the human nuclear RNase P proteins RPP21, RPP29, RPP30, POP5, and RPP38/L7Ae. From these, two heterodimeric pairs are formed in solution: one between RPP21 and RPP29 and one between POP5 and RPP30 [18, 19]. Representative structures of each of these proteins have been determined by nuclear magnetic resonance (NMR) spectroscopy and x-ray crystallography from the hyperthermophilic archaea *Pyrococcus horikoshii* (*Pho*), *Methanocaldoccus jannaschii* (*Mja*), or *Pfu* [20-24]. Furthermore, the structures of the RPP21-RPP29 complex and of the POP5-RPP30 complex have been determined [18, 25]. The *Pfu* RPR contains two separately-folding domains [26] and is

homologous to the bacterial A-type RPR [27], but details of its three-dimensional structure are not yet known.

APPROACH

EPD Reaction and the Selection of Metal Ions

With the knowledge that substantial structural information is already available about structures of components of *Pfu* RNase P, the purpose of this study is to implement a method to provide structural information on the overall organization of subunits in the *Pfu* RNase P holoenzyme. The strategy employed involves the strategic attachment of an ethylenediaminetetraacetic acid (EDTA) moiety to engineered cysteine residues on mutant versions of one of the protein subunits. The EDTA moiety can chelate an array of transition metals and thus facilitate certain structural measurements. Specifically, EDTA-2-aminoethyl 2-pyridyl disulfide (EPD) has previously been used to attach metal ions to cysteine residues (Figure 1) in order to provide protein-nucleic acid and protein-protein structural information (including information from bacterial RNase P) [28-34]. RPP29 was selected as the initial protein target for the addition of the EDTA moiety because, at the time, the interface of the RPP21-RPP29 heterodimer in solution was in need of refinement and these experiments had the potential to provide additional structural information in an effort to improve the accuracy of the structural model [Xu and Foster, unpublished]. Manganese(II) (Mn^{2+}) was chosen as one of the metals to chelate with the EDTA moiety because it is paramagnetic and can therefore enable paramagnetic relaxation enhancement (PRE) NMR experiments [34]. Iron(III) (Fe^{3+}) was also selected because of EDTA-Fe's ability to generate hydroxyl radicals, which can cleave nucleic acid in a distance-dependent manner and therefore facilitate RNA footprinting assays with the RPR and the RPPs [28-30]. EDTA binds both Mn^{2+} and Fe^{3+} tightly: the respective K_ds are $\sim 10^{-11}$ M and $\sim 10^{-21}$ M [35].

PRE NMR and the Generation of Distance Restraints

The nuclei of certain atoms (isotopes), such as those from ^{1}H and ^{15}N, have magnetic dipoles. When exposed to an external magnetic field (such as that provided by the superconducting magnet of an NMR spectrometer), these magnetic dipoles can be thought of as assuming one of two orientations where each orientation is associated with a unique energy level. Irradiating these nuclei with pulses of electromagnetic radiation in the radio-wave range can cause their magnetic dipoles to transition between energy levels. The postulates of quantum mechanics dictate that these transitions to an excited state occur only if the energy (frequency) of the electromagnetic radiation matches the energy difference between the transitional states. It is these transitions that give rise to observable NMR signals [36].

A nucleus in an excited state can be manipulated to expel the excitation (magnetization) to other nuclei, and the resonance frequency of each nucleus through which the magnetization is passed can be measured in an NMR experiment. Signals that link the frequencies of each of those nuclei can be obtained, and such correlation spectra allow for the unambiguous assignment of a signal to its corresponding nuclei [36].

The NMR data included in this study are heteronuclear single-quantum coherence (HSQC) spectra, in which signals arise from through-bond correlation between each ^{1}H-^{15}N bonded pair in the protein. Each of these signals is a sensitive probe of the local chemical environment that surrounds the ^{1}H-^{15}N pair. Among other uses, the ^{15}N-HSQC experiment is helpful in determining whether a protein is folded or whether a series of mutations has dramatically altered the tertiary structure of a protein [36]. In other words, the ^{15}N-HSQC spectrum can provide a high-resolution “fingerprint” of the protein [35].

As opposed to the HSQC NMR experiment, 2D nuclear Overhauser effect spectroscopy (NOESY) experiment can correlate two protons if they are within 5-6 Å of each other through space [36]. These correlations can provide useful short-range structural information and are the principal structural measurement in NMR-based structure determination of proteins. Paramagnetic relaxation enhancement (PRE) NMR experiments can provide complementary longer-range structural information (up to 35 Å for a Mn^{2+}-^{1}H interaction) [38]. During relaxation of an NMR signal, magnetization is lost as the excited states of the nuclei lose enthalpy or gain entropy [37]. In PRE experiments performed with Mn^{2+}, such as in this study, the introduction of a Mn^{2+} ion to a system causes an enhancement of these nuclear relaxation processes due to through-space interactions with the large magnetic moment of the unpaired Mn^{2+} electrons [37]. Therefore, intensities of NMR signals that arise from sites near the Mn^{2+} ion decrease in a quantifiable, distance-dependent manner. If these signals are well separated and have been assigned to individual positions in the molecule, distances from the NMR nuclei to the paramagnetic probe can be calculated from the reduced intensity.

RNA Footprinting and the Fenton Reaction

Whereas PRE NMR experiments can provide valuable structural information, they are limited by the requirement of assigned, well-resolved NMR signals. However, the same functionalized proteins used for PRE NMR can be used to provide protein-RNA structural information in footprinting experiments that lead to RNA cleavage in the vicinity of the metal probe. The Fenton reaction was utilized to complete the RNA footprinting experiments [39]. EDTA-Fe creates hydroxyl radicals from water molecules when it is in the presence of ascorbate and hydrogen peroxide and has previously been used to obtain high-resolution structural information about the *E. coli* RNase P holoenzyme [30]. In this study, the *Pfu* RPR was

incubated alongside the EDTA-Fe moiety and was cleaved in a distance-dependent manner by the hydroxyl radicals. Reverse-transcribed complementary DNA (cDNA) fragments partially synthesized with radiolabeled dideoxynucleoside triphosphates (ddNTPs) were then subjected to polyacrylamide gel electrophoresis and visualized by autoradiography, thus indicating the cleavage site on the RNA [30].

Single-cysteine Mutants and the Selection of Sites

To ensure precise placement of the EDTA moiety, it is useful to have only one cysteine residue per protein. Wild type RPP21 has a zinc atom that is bound by four cysteine residues and this interaction helps to stabilize the protein's tertiary structure [40, 18]. Therefore, RPP29 provided a better target for the modification reaction because its cysteine residue was deemed to be less essential to the structure and function of the protein. In RPP29, the wild-type cysteine is located at residue 94 and is buried in the interior of the protein when RPP29 forms its native complex with RPP21 [18]. Modifying surface-exposed residues in the native structural conformation is preferred to modifying buried residues because surface residues are more easily accessed by the EPD reagent. Additionally, the EDTA moiety from EPD is hydrophilic and the modification of surface residues would likely perturb the overall structure less than would the modification of buried residues.

The native cysteine was therefore mutated to alanine and a library of single-cysteine mutants was eventually developed [Xu and Foster, unpublished]. These mutants included R75C/C94A (henceforth known as R75C) and K88C/C94A (henceforth known as K88C), among others. Positively-charged amino acids were targeted as the sites of cysteine mutation due to their relatively high probability of being near or in the protein-RNA binding interface; due to the

distance-dependent manner of hydroxyl cleavage, positioning the EDTA-Fe moiety near the protein-RNA interface is vital if cleavage of the RNA is desired.

Prior to the PRE NMR and the RNA footprinting experiments, it was important to perform activity assays to ensure that the modification of the RPP29 proteins did not render the proteins non-functional. In these assays performed by members of the Gopalan laboratory, the *Pfu* holoenzyme was reconstituted and incubated with radiolabeled ptRNA substrate. After incubation, reaction products were run on a polyacrylamide gel and visualized with a phosphorimager to quantify the reconstituted enzyme activities.

MATERIALS AND METHODS

Generation of a Single-cysteine Library

Mutant pET-33b(+) plasmids encoding the *Pfu* RPP29 gene under control of the T7 promoter, and resistant to the antibiotic kanamycin, were engineered via QuikChange mutagenesis and verified by DNA sequencing [Xu and Foster, unpublished].

Expression of RPP29

RPP29 proteins were produced based on procedures described in [18]. For all of the RPP29 mutants, the plasmid of interest was transformed by electroporation into *E. coli* BL21(DE3) Rosetta cells (Novagen), a bacterial strain that expresses rare tRNAs from a plasmid that encodes resistance to the antibiotic chloramphenicol. Lysogeny broth (LB) was then added and the cells were incubated at 37 °C for one hour before being plated on an LB/agar plate that contained the antibiotics kanamycin (30 μg/L) and chloramphenicol (34 μg/L). After incubation at 37 °C for 12-16 hours, a single colony was harvested from the plate and placed in a starter culture containing 100 mL of LB, 30 μg/L of kanamycin, and 34 μg/L of chloramphenicol. This starter culture was shaken at 250 rotations per minute (RPM) for 12 hours at 37 °C. Afterwards, 12.5 mL of the starter culture was added to each of two 500-mL solutions of LB broth in 2-L Erlenmeyer flasks (with 30 μg/L of kanamycin and 34 μg/L of chloramphenicol). These Erlenmeyer flasks were shaken at 250 RPM and 37 °C until the OD_{600} reached 0.6. (For protein to be labeled with ^{15}N instead of LB media, two 500-mL solutions of minimal media, each containing 3.3 g anhydrous Na_2HPO_4, 1.5 g KH_2HPO_4, 0.25 g NaCl, and 0.5 g $^{15}NH_4Cl$, were placed in 2-L Erlenmeyer flasks. 5 mL of the starter culture was then added to each of the flasks with minimal media and shaken at 250 RPM and 37 °C until the OD_{600} reached 0.6.) At this

point, 1 mM isopropyl β-D-1-thiogalactopyranoside (IPTG) was added to both flasks to induce protein expression and the flasks were shaken at 250 RPM and 37 °C for four hours. Cells were then harvested by centrifugation at 6,084 g and 15 °C for 10 minutes.

Purification of RPP29 Derivatives

Aqueous buffers used during the purification:

Native Buffer	Resuspension Buffer
25 mM Tris-HCl, pH 7.5	25 mM Tris-HCl, pH 7.5
1 mM EDTA	1 mM EDTA
0.1 mM PMSF*[#]	0.1 mM PMSF*
50 mM Dithiothreitol (DTT)*	50 mM DTT*
0.02 % NaN_3	7 M Urea
	0.02 % NaN_3

Buffer A1	Buffer B1
25 mM Tris-HCl, pH 7.0	25 mM Tris-HCl, pH 7.0
25 mM KCl	2 M KCl
10 mM DTT*	10 mM DTT*
7 M Urea	7 M Urea
0.02 % NaN_3	0.02 % NaN_3

* = freshly added (just before use)
# = phenylmethanesulfonylfluoride

The cell pellets from the two 500-mL cultures were combined and resuspended in 30 mL of Native Buffer and then lysed by sonication on ice [five second pulse, two second rest, six minutes, 65 watts]. These lysed cells were then centrifuged at 7,649 g and 15 °C for 15 minutes. The pellet from this centrifugation step was then resuspended in 30 mL of Resuspension Buffer and sonicated on ice [five second pulse, two second rest, six minutes, 65 watts]. After centrifugation at 7,649 g and 15 °C for 15 minutes, the supernatant was filtered (0.45 μm) and then passed through a 5-mL SP cation-exchange column previously equilibrated with 25 mL of Resuspension Buffer (with 10 mM DTT and 1 mM PMSF). This SP column was then attached to

a fast protein liquid chromatography (FPLC) instrument with Buffer A1 and Buffer B1. In the first segment of the elution gradient, the composition of the elution buffer changed from 0 % Buffer B1 to 10 % Buffer B1 over five column volumes (CVs). During the second segment of the gradient, the composition of the elution buffer changed from 10 %B to 25 %B over 10 CVs. During the third segment of the gradient, the composition of the elution buffer changed from 25 % Buffer B1 to 100 % Buffer B1 over two CVs. During the final segment of the gradient, the composition of the elution buffer was 100 % Buffer B1. The protein typically eluted at a KCl concentration of about 300 mM, corresponding to an elution buffer composition of about 14 % Buffer B1. Using this protocol, the R75C and K88C proteins were expressed and purified.

EPD Modification Reaction to Prepare NMR Samples

First, 10 mM DTT was added to the sample of protein to be modified to ensure reduction of the cysteine residues. This protein solution was then passed through a PD-10 desalting column (GE Healthcare) into a buffer with 10 mM Tris, 10 mM KCl, 0.02 % NaN_3, and pH 8.0. Each pass through a PD-10 column dilutes the protein concentration by a factor of 5/7 because 2.5 mL of protein sample are loaded into the column and 3.5 mL are used to elute. After determining the concentration of the protein in solution by using its predicted extinction coefficient at 280 nm [41], EPD was added to the solution in five-fold excess over the protein concentration. This solution was then passed through another PD-10 column into a buffer with 10 mM Tris, 10 mM KCl, 0.02 % NaN_3, and pH 8.0. Manganese(II) (as manganous sulfate) was then added in a five-fold excess over the protein concentration. Excess manganese was finally removed by using a HiTrap Desalting Column (Sigma-Aldrich) connected to the FPLC machine to exchange the old buffer for one with 10 mM Tris, 10 mM KCl, 0.02 % NaN_3, and pH 8.0. The protein sample (RPP29-EDTA-Mn^{2+}) was then concentrated by ultrafiltration with a 3-kDa molecular weight

cutoff membrane (Amicon) in preparation for the NMR experiments. Final protein concentrations ranged from 172 μM to 315 μM.

EPD Modification Reaction to Prepare Samples for RNA Footprinting

EPD was reacted with a 10-fold excess of $FeCl_3$ in water that had been run through a Chelex-100 column. Protein cysteine residues were reduced by addition of 10 mM DTT to the sample of protein to be modified. A three-step dialysis procedure into a 1000-mL solution with 10 mM Tris, 10 mM KCl, 0.02 % NaN_3, and pH 8.0 was performed on the ~2-mL protein samples, with each step lasting one hour. After the last step of the dialysis procedure, the previously-prepared EPD-Fe^{3+} was added in a 10-fold excess to the concentrations of the RPP29 mutants. These modified protein samples were then stored at 4 °C until being used for the footprinting assays.

Quantification of the Extent of EPD Modification

Ellman's reagent (Pierce Biotechnology); 5,5'-dithio-bis-(2-nitrobenzoic acid) (DTNB); which quantifies the concentration of free thiol groups in solution, was used to quantify the extent of the EPD modification (Figure 2) [42, 43]. The reaction of DTNB with cysteine thiol groups is monitored by observing the production of 2-nitro-5-thiobenzoic acid (TNB), which has an extinction coefficient of 14,150 $M^{-1}cm^{-1}$ at 412 nm. The reaction was carried out in a buffer with 10 mM Tris, 10 mM KCl, 0.02 % NaN_3, and pH 8.0. A standard curve that plotted the absorbance of 412 nm light against the concentration of various stock solutions of cysteine was generated and used to determine thiol concentrations (data not shown).

Preparation of NMR Samples

Concentrated, uniformly-^{15}N-labeled K88C-EDTA ([U-^{15}N]-K88C-EDTA) and [U-^{15}N]-K88C-EDTA-Mn^{2+} species were generated as outlined above. Afterward, 4,4-dimethyl-4-silapentane-1-sulfonic acid (DSS) was added in a five-fold excess over the protein concentration and deuterium oxide (D_2O) was added to 5% (v/v). The sample was then loaded into a reduced-volume NMR tube (Shigemi, Inc.) and stored at 4 °C.

Acquisition of NMR Data

NMR spectra were recorded at 53 °C on an 800 MHz Bruker Avance DRX spectrometer (Billerica, MA) located on the main campus of The Ohio State University and equipped with triple resonance pulse-field gradient probes. NMR data were processed and analyzed with NMRPipe and NMRViewJ [44, 45]. The resulting spectra were compared to the assigned ^{15}N-HSQC spectrum of the wild type RPP29 protein [46].

Activity and Footprinting Assays

Results of RNase P activity assays and hydroxyl radical-mediated footprinting studies were obtained in the Gopalan laboratory by Cecilia Go and Dr. Lien Lai, respectively. RPP29-EDTA-Fe^{3+} (K88C-EDTA-Fe^{3+}, for example) was generated as outlined above. This modified RPP29 protein was reconstituted with the other *Pfu* RNase P subunits, including the RPR, and then incubated with labeled ptRNA substrate. Activity of each mutant was determined by the initial reaction velocities. For the footprinting assays, modified RPP29 was incubated with RPR and introduced to ascorbate and hydrogen peroxide to promote the formation of hydroxyl radicals [30]. Radiolabeled, reverse-transcribed cDNA fragments were then run on a polyacrylamide gel and used to map cleavage sites to the RPR.

RESULTS

Single-cysteine mutants of R75C and K88C were over-expressed in *E. coli* and then purified. After reacting K88C protein with EPD, an assay with Ellman's reagent showed that greater than 98% of the cysteine residues had been modified by EPD (Table 1). Additionally, K88C, K88C-EDTA, and K88C-EDTA-Mn^{2+} species were analyzed by electrospray ionization (ESI) mass spectrometry to verify their identities (Figure 4). Interestingly, the mass spectra showed evidence of protein carbamylation, which is commonly seen if old or previously-heated solutions of urea are used in protein purifications [46-48]. Cyanate ions resulting from urea degradation can react with lysine residues to form homocitrulline, a chemical modification that would result in a protein mass increase of 43 Daltons (Da). Moreover, the three most-abundant peak distributions in panel (B) of Figure 4 show evidence of metal contamination: the distribution with a mass-to-charge (m/z) ratio centered around 15,245.06 is likely the K88C-EDTA species, whose expected average mass is 15,245.5 Da. The peak distribution with an m/z ratio centered around 15,306.96 could correspond to K88C-EDTA species that had chelated a transition metal with an approximate mass of 62 Da. Examples of such metals include cobalt (~59 Da), nickel (~59 Da), copper (~64 Da), and zinc (~65 Da). Therefore, this peak distribution could contain many different metals that were chelated by the K88C-EDTA species prior to the introduction of manganese. For completeness, the peak distribution with an m/z ratio centered around 15,349.97 could represent the K88C-EDTA species that was both modified by cyanate and contaminated with a transition metal.

In preparation for the NMR experiments, the K88C mutant of RPP29 (uniformly labeled with ^{15}N) was over-expressed in *E. coli* and then purified with a yield of approximately 115 mg per liter of minimal media (Figure 3). Purified [U-^{15}N]-K88C was then modified with EPD

(resulting in [U-^{15}N]-K88C-EDTA) and then mixed with Mn^{2+} to generate the [U-^{15}N]-K88C-EDTA-Mn^{2+} species. Figures 5-8 show NMR spectra of wild type [U-^{15}N]-RPP29, [U-^{15}N]-C94A, [U-^{15}N]-K88C/C94A ("K88C"), [U-^{15}N]-K88C/C94A-EDTA ("K88C-EDTA"), and [U-^{15}N]-K88C-EDTA-Mn^{2+} (K88C-EDTA-Mn^{2+}). The NMR experiments involving the [U-^{15}N]-K88C-EDTA and [U-^{15}N]-K88C-EDTA-Mn^{2+} species examined the effects of adding Mn^{2+} to the protein sample. Residues whose peaks showed the highest sensitivity to the PRE probe were mapped to the structure of *Pfu* RPP29 based on assignments for the C94A mutant (Figure 9): residues V64, Y63, T74, V86, W87, V89, and K91 were found to be most broadened.

In preparation for the RNA footprinting experiments, unlabeled K88C protein was over-expressed in *E. coli* and then purified with a yield of approximately 80 mg per liter of LB (Figure 10). The R75C mutant was also over-expressed and purified in the same manner. Both proteins were then modified with EPD-Fe that had previously been mixed to generate the respective RPP29-EDTA-Fe^{3+} species. The K88C and K88C-EDTA-Fe^{3+} species were subjected to analysis by matrix assisted laser desorption/ionization (MALDI) mass spectrometry to verify their respective identities (Figure 11). Precursor tRNA cleavage assays were used to check the activity of the RPP29 mutants in the context of the complete holoenzyme (data not shown). RNA footprinting assays were then performed on both RPP29 mutants and reverse-transcribed cDNA fragments from the assays were run on a polyacrylamide gel (Figure 12). After analyzing the polyacrylamide gel, the cleavage sites were mapped to the primary and secondary structures of the RPR (Figure 13). Modified R75C and K88C mutants were shown to footprint on P9 of the *Pfu* RPR; cleavage sites from the footprinting assays were in regions of the RPR that have previously been predicted to bind RPP29 [18].

Discussion

In preparation for the PRE NMR experiments, K88C was successfully purified from BL21(DE3) Rosetta cells and was relatively straightforward. The EDP modification reaction, however, proved to be somewhat complicated. K88C, being a single-cysteine mutant of RPP29, can assemble covalent dimers by forming disulfide bonds. Since the thiol groups on the cysteine residues are necessary for the EPD modification reaction, it is important to limit the formation of these inter-protein disulfide bonds by using a reducing agent (such as dithiothreitol, DTT). In a type of Catch-22, the reducing DTT species cannot be present during the modification reaction, or else it will cleave the disulfide bond on DTNB and also reduce any disulfide bonds formed as a result of the EPD modification reaction. It should further be noted that the longer RPP29 is in solution in a reduced form under oxidizing conditions (i.e., without reducing agents), the more inter-protein disulfide bonds it will form; protein oxidation has been shown to be spontaneous [50].

Therefore, to overcome this challenge, protein reduction by DTT, followed by three rapid rounds of dialysis to remove the DTT, was first attempted. This technique was met with little success: the EPD reagent would react (as determined by Ellman's reagent) repeatedly in excess of the known protein concentration (as determined by UV-Vis spectroscopy and the protein's predicted extinction coefficient at 280 nm), suggesting residual DTT contamination. As an alternative to dialysis, PD-10 desalting columns allowed for the rapid removal of DTT and enabled the EPD modification reaction to attach the EDTA moiety to RPP29.

To verify the successful addition of the EDTA moiety to the RPP29 mutants, a number of methods were examined. The extinction coefficient of 2-pyridylthiol, the leaving group from the EPD modification reaction, is known at 343 nm and could hypothetically be used to monitor the

progress of the modification reaction [51]. However, simply reporting on the cleavage of the disulfide bond in EPD, as this assay would do, would not ensure that the EDTA moiety has been properly attached to the cysteine residues of interest. Therefore, in addition to monitoring the progress of the modification reaction at 343 nm, two additional verification methods were employed. First, Ellman's reagent was used to check the concentration of free thiol species in solution after the EPD modification reaction. This test would detect any unreacted cysteine residues, so ideally Ellman's reagent would report no free thiol groups in solution after the reaction.

As the second method of verifying the successful attachment of the EDTA moiety, two forms of mass spectrometry (ESI and MALDI) were employed. ESI analysis of K88C samples resulted in some interesting mass spectra. All three spectra show evidence of lysine carbamylation, a phenomenon commonly encountered if protein samples have been purified with old urea or urea that has been heated [47-49]. Incidentally, the buffers with urea that were used for that purification of RPP29 were nine months old at the time of the purification and had been accidentally boiled while being made. In addition to this lysine carbamylation, however, there was also evidence of metal contamination.

NMR experiments were performed on the [U-^{15}N]-K88C-EDTA and [U-^{15}N]-K88C-EDTA-Mn^{2+} species and resulted in the mapping of signals affected by PRE to residues on RPP29. Protein degradation was observed for the [U-^{15}N]-K88C-EDTA sample after 16 days, a result that is consistent with previous studies (Appendix A) [52].

Due to the likely metal contamination of the species with the EDTA moiety, the protocol for adding the metals was altered in future modifications: a Chelex-100 column was used to remove trace metal contaminants from the water used to suspended EPD. In preparation for RNA

footprinting experiments, suspended EPD was then mixed with Fe^{3+} and reacted with the single-cysteine RPP29 mutants. RNA footprinting assays were then conducted with modified RPP29 mutants prepared with this new protocol. Currently, this modification protocol is also being used with other RPPs [Lai, Lai, Foster and Gopalan, unpublished].

CONCLUSION

A technique for the modification of cysteine residues with an EDTA moiety and chelated metal has successfully been implemented with the *Pfu* RPP29 protein. Modification of the RPP29 mutants was verified in multiple ways and used to chelate multiple metals to cysteine residues via an EDTA moiety from EPD. PRE NMR experiments were performed and used to detect residues on K88C that are close to the chelated Mn^{2+}. Residues 86-89 and 91 were found to be closest to the paramagnetic probe, which was expected because the EDTA moiety was attached to residue 88. Therefore, these experiments also provided verification that the structural probe was attached to the desired protein residue. Moreover, RPP29 footprints from RPR cleavage assays were mapped to regions of the RPR that were previously predicted to bind RPP29. These metal chelation techniques, if applied to multiple cysteine residues on multiple subunits of *Pfu* RNase P, could be used to obtain numerous distance restraints that could lead to the development of a three-dimensional, atomic-resolution model of the *Pfu* RNase P holoenzyme.

ACKNOWLEDGEMENTS

The author wishes to thank Dr. Mark P. Foster, Dr. Venkat Gopalan, Dr. Yiren Xu, Dr. Ross Wilson, Ms. Stella M. Lai, Ms. Amber Simmons, Dr. Lien Lai, Dr. Sri Oruganti, Mr. Ian Kleckner, Mr. Elihu Ihms, Mr. John Shimko, Mr. Brandon Crowe, and Mr. David Smith for their extensive guidance, support, and insights. Lastly, this research was made possible by funding from the National Institute of Health.

APPENDIX

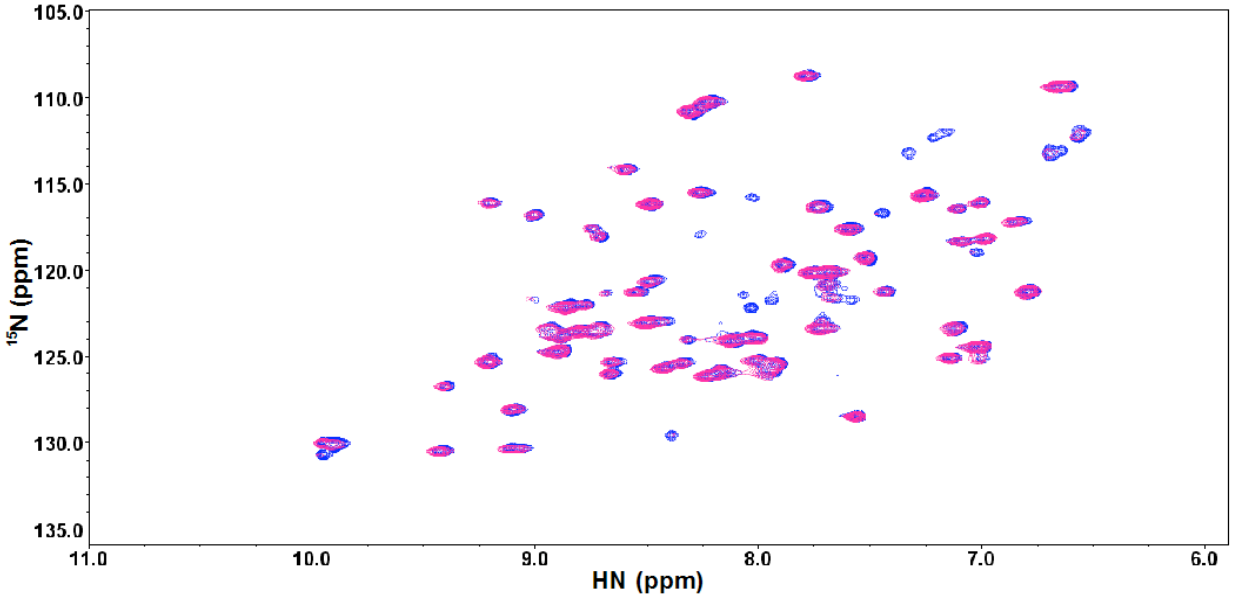

Appendix A. In these overlaid ^{15}N-HSQC spectra, the same [U-^{15}N]-K88C-EDTA sample before and after a 16-day time period is depicted in blue and pink, respectively. The sample was stored at 4 °C during those 16 days. This relatively fast degradation of EPD-modified protein is consistent with previous studies [52].

REFERENCES

1. Hall T. A., Brown, J. W. (2001). The ribonuclease P family. *Methods Enzymol* **341**, 56-77.
2. Hartmann E., Hartmann R. K. (2003). The enigma of ribonuclease P evolution. *Trends Genet* **19**, 561-9.
3. Jarrous N., Altman S. (2001). Human ribonuclease P. *Methods Enzymol* **342**, 93-100.
4. Stark B., Kole R., Bowman E., Altman S. (1978). Ribonuclease P: an enzyme with an essential RNA component. *PNAS* **75**, 3717-3721.
5. Waldrop M. M. (1989). Catalytic RNA wins chemistry Nobel. *Science* **246**, 325.
6. Lai L. B., Chan P. P., Cozen A. E., Bernick D. L., Brown J. W., Gopalan V., Lowe T. M. (2010). Discovery of a minimal form of RNase P in Pyrobaculum. *Proc Natl Acad Sci USA* **107**, 22493-8.
7. Holzmann J., Frank P., Löffler E., Bennett K. L., Gerner C., Rossmanith W. (2008). RNase P without RNA: identification and functional reconstitution of the human mitochondrial tRNA processing enzyme. *Cell* **35**, 462–74.
8. Liu F., Altman S. (1994). Differential evolution of substrates for an RNA enzyme in the presence and absence of its protein cofactor. *Cell*, **77**, 1093-1100.
9. Li Y., Altman S. (2003). A specific endoribonuclease, RNase P, affects gene expression of polycistronic operon mRNAs. *Proc Natl Acad Sci USA* **100**, 13213-13218.
10. Altman S., Wesolowski D., Guerrier-Takada C., Li Y. (2005). RNase P cleaves transient structures in some riboswitches. *Proc Natl Acad Sci USA* **102**, 11284-11289.
11. Mohanty B. K., Kushner S. R. (2008). Rho-independent transcription terminators inhibit RNase P processing of the secG leuU and metT tRNA polycistronic transcripts in Escherichia coli. *Nucleic Acids Res* **36**, 364-375.
12. Chen W-Y., Pulukkunat D. K., Cho I-M., Tsai H-Y., Gopalan V. (2010). Dissecting functional cooperation among protein subunits in archaeal RNase P, a catalytic RNP complex. *Nucleic Acids Res* **38**, 8316–8327.
13. Sun F-J., Caetano-Anolles G. (2010). The ancient history of the structure of ribonuclease P and the early origins of Archaea. *BMC Bioinformatics* **11**, 153.
14. Eubank T., Gopalan V., Biswas R., Javonovic M., Litovchick A., Lapidot A. (2002). Inhibition of bacterial RNase P by aminoglycoside-arginine conjugates. *FEBS lett* **511**, 107-112.
15. Fiala G., Stetter K. O. (1986). Pyrococcus furiosus sp. nov. represents a novel genus of marine heterotrophic archaebacteria growing optimally at 100°C. *Archives of Microbiology* **145**, 56-61.
16. Hartmann E., Hartmann R. K. (2003). The enigma of ribonuclease P evolution. *Trends Genet* **19**, 561–569.
17. Tsai H. Y., Pulukkunat D. K., Woznick W., Gopalan V. (2006). Functional reconstitution and characterization of Pyrococcus furiosus RNase P. *Proc Natl Acad Sci USA* **103**, 16147–16152.
18. Xu Y., Amero C., Pulukkunat D., Gopalan V., Foster M. (2009). Solution structure of an archaeal RNase P binary protein complex: formation of the 30-kDa complex between Pyrococcus furiosus RPP21 and RPP29 is accompanied by coupled protein folding and highlights critical features for protein–protein and protein–RNA interactions. *J Mol Biol* **392**, 1043-1055.

19. Cho, I. M., Lai, L. B., Susanti, D., Mukhopadhyay, B., Gopalan, V. (2010). Ribosomal protein L7Ae is a subunit of archaeal RNase P. *Proc Natl Acad Sci USA* **107**, 14573-8.
20. Wilson, R. C., Bohlen, C. J., Foster, M. P., Bell, C. E. (2006). Structure of Pfu Pop5, an archaeal RNase P protein. *Proc Natl Acad Sci USA* **103**, 873-8.
21. Amero, C. D., Boomershine, W. P., Xu, Y., Foster, M. (2008). Solution structure of Pyrococcus furiosus RPP21, a component of the archaeal RNase P holoenzyme, and interactions with its RPP29 protein partner. *Biochemistry* **47**, 11704-10.
22. Boomershine, W. P., McElroy, C. A., Tsai, H. Y., Wilson, R. C., Gopalan, V., Foster, M. P. (2003). Structure of Mth11/Mth Rpp29, an essential protein subunit of archaeal and eukaryotic RNase P. *Proc Natl Acad Sci USA* **100**, 15398-403.
23. Takagi, H., Watanabe, M., Kakuta, Y., Kamachi, R., Numata, T., Tanaka, I., Kimura, M. (2004). Crystal structure of the ribonuclease P protein Ph1877p from hyperthermophilic archaeon Pyrococcus horikoshii OT3. *Biochem Biophys Res Commun* **319**, 787-94.
24. Suryadi J., Tran E. J., Maxwell E. S., Brown B. A. (2005). The crystal structure of the Methanocaldococcus jannaschii multifunctional L7Ae RNA-binding protein reveals an induced-fit interaction with the box C/D RNAs. *Biochemistry* **44**, 9657–9672.
25. Kawano, S., Nakashima, T., Kakuta, Y., Tanaka, I., Kimura, M. (2006). Crystal structure of protein Ph1481p in complex with protein Ph1877p of archaeal RNase P from Pyrococcus horikoshii OT3: implication of dimer formation of the holoenzyme. *J Mol Biol* **357**, 583-91.
26. Pulukkunat, D. K., Gopalan, V. (2008). Studies on Methanocaldococcus jannaschii RNase P reveal insights into the roles of RNA and protein cofactors in RNase P catalysis. *Nucleic Acids Res* **36**, 4172-80.
27. Kazantsev A. V., Krivenko A. A., Harrington D. J., Holbrook S. R., Adams P. D., Pace N. R. (2005). Crystal structure of a bacterial ribonuclease P RNA. *Proc Natl Acad Sci USA* **102**, 13392-13397.
28. Platis I. E., Ermácora M. R., Fox R. O. (1993). Oxidative polypeptide cleavage mediated by EDTA-Fe covalently linked to cysteine residues. *Biochemistry* **32**, 12761-12767.
29. Ermácora M. R., Ledman D. W., Hellinga H. W., Hsu G. W., Fox R. O. (1994). Mapping staphylococcal nuclease conformation using an EDTA-Fe derivative attached to genetically engineered cysteine residues. *Biochemistry* **33**, 13625-13641.
30. Biswas R., Ledman D. W., Fox R. O., Altman S., Gopalan V. (2000). Mapping RNA-protein interactions in ribonuclease P from Escherichia coli using disulfide-linked EDTA-Fe. *J Mol Biol* **296**, 19-31.
31. Dvoretsky A., Gaponenko V., Rosevear, P. R. (2002). Derivation of structural restraints using a thiol-reactive chelator. *FEBS Lett* **528**, 189–192.
32. Gaponenko V., Altieri A.S., Li J., Byrd R.A. (2002). Breaking symmetry in the structure determination of (large) symmetric protein dimmers. *J Biomol NMR* **24**, 143–148.
33. Gaponenko V., Sarma S.P., Altieri A.S., Horita D.A., Li J., Byrd R.A. (2004). Improving the accuracy of NMR structures of large proteins using pseudocontact shifts as long-range restraints. *J Biomol NMR* **28**, 205–212.
34. Pintacuda G., Moshref A., Leonchiks A., Sharipo A., Otting G. (2004). Site-specific labelling with a metal chelator for protein-structure refinement. *J Biomol NMR* **29**, 351-361.
35. Iwahara J., Anderson D. E., Murphy E. C., Clore G. M. (2003). EDTA-derivatized deoxythymidine as a tool for rapid determination of protein binding to DNA by intermolecular paramagnetic relaxation enhancement. *J Am Chem Soc* **125**, 6634-6635.

36. Kwan A. H., Mobli M., Gooley P. R., King G. F., Mackay J. P. (2011). Macromolecular NMR spectroscopy for the non-spectroscopist. *FEBS J* **278**, 687-703.
37. Bieri M., Kwan A. H., Mobli M., King G. F., Mackay J. P., Gooley P. R. (2011). Macromolecular NMR spectroscopy for the non-spectroscopist: beyond macromolecular solution structure determination. *FEBS J* **278**, 704-715.
38. Iwahara J., Schwieters C. D., Clore G. M. (2004). Ensemble approach for NMR structure refinement against ^{1}H paramagnetic relaxation enhancement data arising from a flexible paramagnetic group attached to a macromolecule. *J Am Chem Soc* **126**, 5879-5896.
39. Fenton H. J. (1894). Oxidation of tartaric acid in presence of iron. *Chem Soc* **65**, 899-910.
40. Boomershine W. (2005). Structure and interactions of archael RNase P proteins *Mth* Rpp29 and *Pfu* Rpp21. Ph.D dissertation, Department of Biochemistry, The Ohio State University, Columbus, OH.
41. Gasteiger E., Hoogland C., Gattiker A., Duvaud S., Wilkins M. R., Appel R.D., Bairoch A. (2005). "Protein Identification and Analysis Tools on the ExPASy Server." John M. Walker (ed): *The Proteomics Protocols Handbook*, Humana Press. pp. 571-607.
42. Ellman, G. (1959). Tissue sulfhydryl groups. *Archieves in Biochemistry and Biophysics* **82**, 70-77.
43. Riddles P. W., Blakeley R. L., Zerner B. (1983). Reassessment of Ellman's reagent. *Meth Enzymol* **91**, 49-60.
44. Delaglio F., Grzesiek S., Vuister G. W., Zhu G., Pfeifer J., Bax A.(1995). NMRPipe: a multidimensional spectral processing system based on UNIX pipes. *J Biomol NMR* **6**, 277–293.
45. Johnson B. A. (2004). Using NMRView to visualize and analyze the NMR spectra of macromolecules. *Methods Mol Biol* **278**, 313–352.
46. Xu Y. (2009). Structure and interactions of archaeal RNase P proteins: RPP29 and RPP21. Ph.D dissertation, Department of Biochemistry, The Ohio State University, Columbus, OH.
47. Stark G. R., Stein W. H., Moore S. (1960). Reactions of the cyanate present in aqueous urea with amino acids and proteins. *The Journal of Biological Chemistry* **235**, 3177-3181.
48. Dorrestein P. C., Kelleher N. L. (2006). Dissecting non-ribosomal and polyketide biosynthetic machineries using electrospray ionization fourier-transform mass spectrometry. *Nat Prod Rep* **23**, 893-918.
49. Ebright Y. W., Chen Y., Pendergrast P. S., Ebright R. H. (1992). Incorporation of an EDTA-metal complex at a rationally selected site within a protein: application to EDTA-iron DNA affinity cleaving with catabolite gene activator protein (CAP) and Cro. *Biochemistry* **31**, 10664-10670.
50. Anfinsen C. B., Haber E. (1961). Studies on the reduction and re-formation of protein disulfide bonds. *J Biol Chem* **236**, 1361-1363.
51. Högemann D., Josephson L., Weissleder R., Basilion J. P. (2000). Improvement of MRI probes to allow efficient detection of gene expression. *Bioconjugate Chem* **11**, 941-946.
52. Iwahara J., Tang C., Clore G. M. (2007). Practical aspects of 1H transverse paramagnetic relaxation enhancement measurements on macromolecules. *Journal of Magnetic Resonance* **184**, 185-195.
53. Ebright Y. W., Chen Y., Pendergrast P. S., Ebright R. H. (1992). Incorporation of an EDTA-metal complex at a rationally selected site within a protein: application to EDTA-iron

DNA affinity cleaving with catabolite gene activator protein (CAP) and Cro. *Biochemistry* **31**, 10664-10670.
54. Pierce, "Ellman's Reagent."

FIGURES

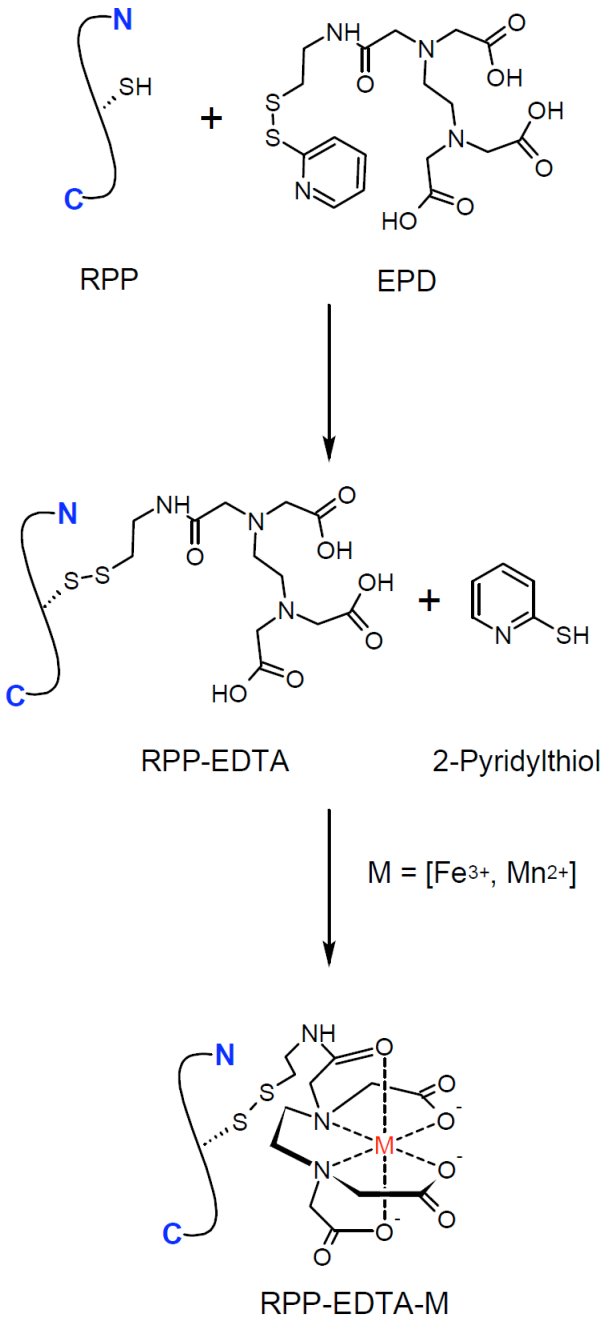

Figure 1. EPD enables the attachment of an EDTA moiety to a cysteine thiol group and 2-pyridylthiol is produced as the leaving group. The RPP-EDTA species can then chelate an array of multivalent transition metals. Figure adapted from reference [28]. If fully extended, the length of the EDTA moiety from the cysteine's α carbon to the metal ion is 14 Å [53].

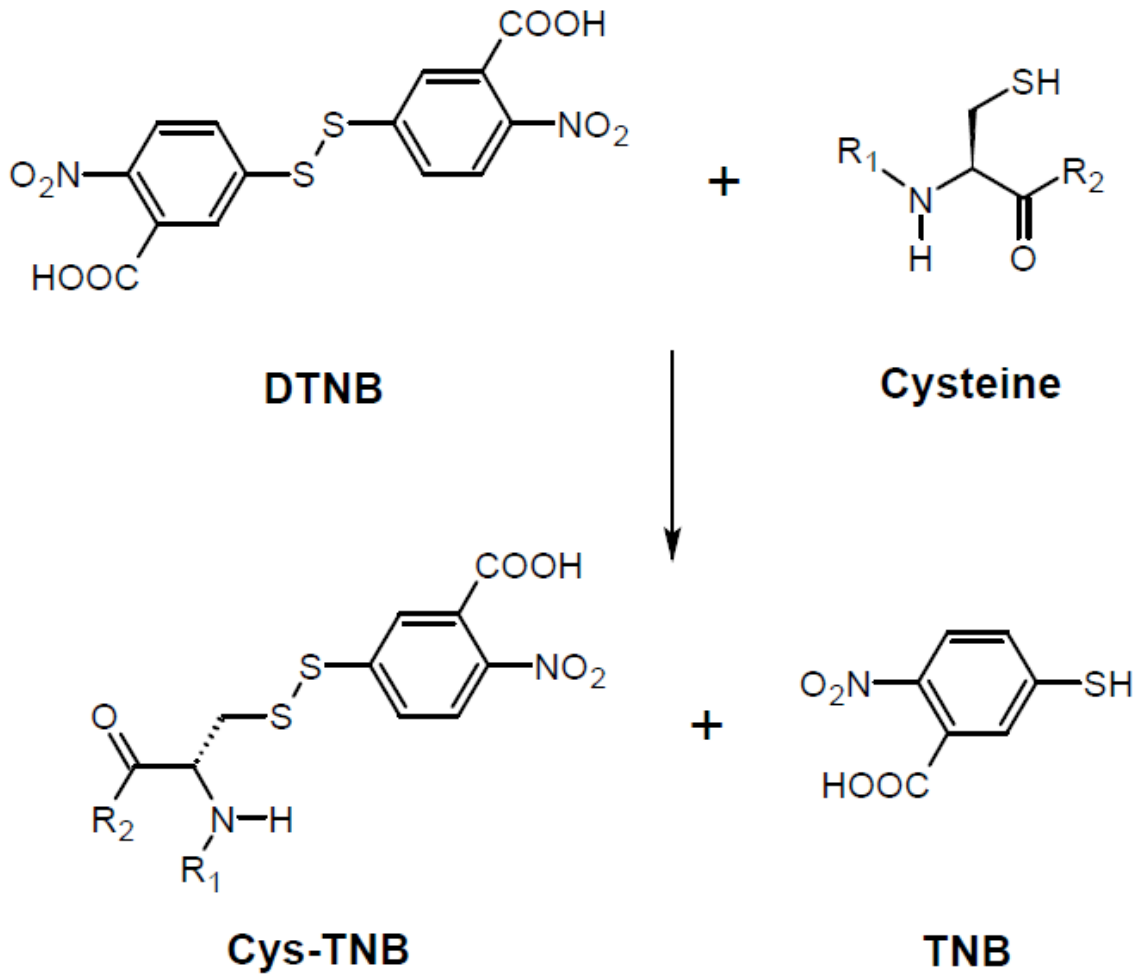

Figure 2. Ellman's reagent quantifies free thiol concentrations: DTNB reacts with thiol groups, such as that attached to the β carbon of cysteine residues. The production of TNB can be monitored at 412 nm and is related to the concentration of free thiol groups by a 1:1 ratio (assuming there are no reducing agents in the assay). Figure adapted from reference [43].

(A)

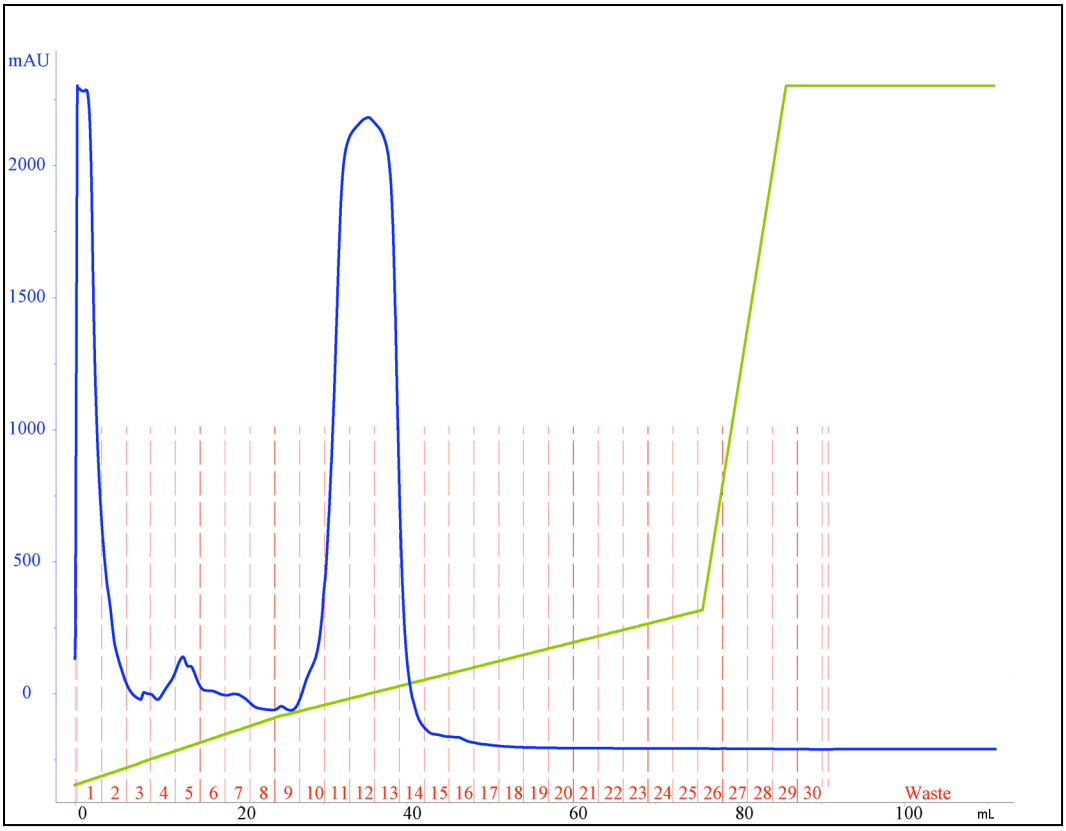

(B)

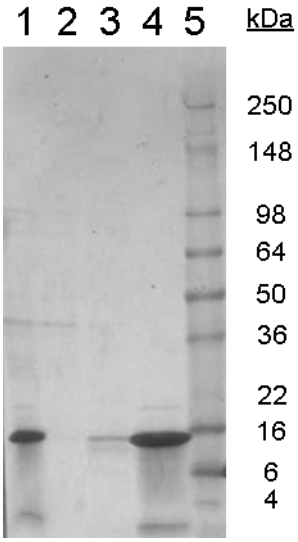

Figure 3. Purification of ^{15}N-labeled K88C protein for NMR experiments with a 5-mL SP column. **(A)** In this FPLC chromatogram, the green curve represents the volume percent of Buffer B that is in the column. About half of the protein has eluted by the time the [KCl] reaches 300 mM, which is around 14 % Buffer B. The blue curve represents the UV absorbance at 280 nm of the eluting material from the column, and the dashed, red line segments delineate the different eluate fractions; fractions 11-13 contained the K88C protein. **(B)** In this 4-20 % Tris-HCl SDS-PAGE gel (Bio-Rad, stained with Coomassie Brilliant Blue dye), lane one is the SP column load-on, lane two is the SP column flow-through, lane three is fraction five from the FPLC run, lane four is combined fractions 11-13 from the FPLC run, and lane five is the SeeBlue Plus2 Pre-Stained Standard protein ladder.

Table 1. Ellman's reagent quantifies the extent of EPD modification of K88C.

Quantification Method	Absorbance Before Modification	Calculated [K88C] Before Modification	Absorbance After Modification	Calculated [K88C] after Modification
Extinction (A_{280})	0.313	0.209 mM	0.221	0.148 mM
Ellman's (A_{412})	0.262	0.208 mM	0.003	0.002 mM

Quantification of [K88C] was performed (by two methods) before and after EPD modification. The protein's predicted extinction coefficient of 37,470 $M^{-1}cm^{-1}$ at 280 nm [41] was used in conjunction with an Ellman's reagent assay that monitored the production of TNB, whose extinction coefficient at 412 nm is 14,150 $M^{-1}cm^{-1}$. Absorbance readings at 280 nm were first blanked with a buffer with 20 mM phosphate, 6 M guanidine-HCl, and pH 6.5. 40 uL of the unmodified K88C sample was combined with 960 uL of the buffer used for the blank and the absorbance at 280 nm was measured. Ellman's reagent was used to determine the concentration of free thiol species according to the protocol in [54] (except the reaction buffer was 10 mM KCl, 10 mM Tris, pH 8.0). Both methods of quantification calculated similar [K88C] concentrations before modification. The same set of experiments was performed after EPD modification. This time, the calculated concentration of K88C from Ellman's reagent was much lower than the calculated K88C concentration from the protein extinction coefficient. Note that the PD-10's diluting factor of 5/7 accounts for the decrease in calculated K88C concentration by the A_{280} method. The difference in the calculated K88C concentrations after EPD modification suggests that 0.146/0.148 = 98.6 % of the cysteine residues have been modified by EPD.

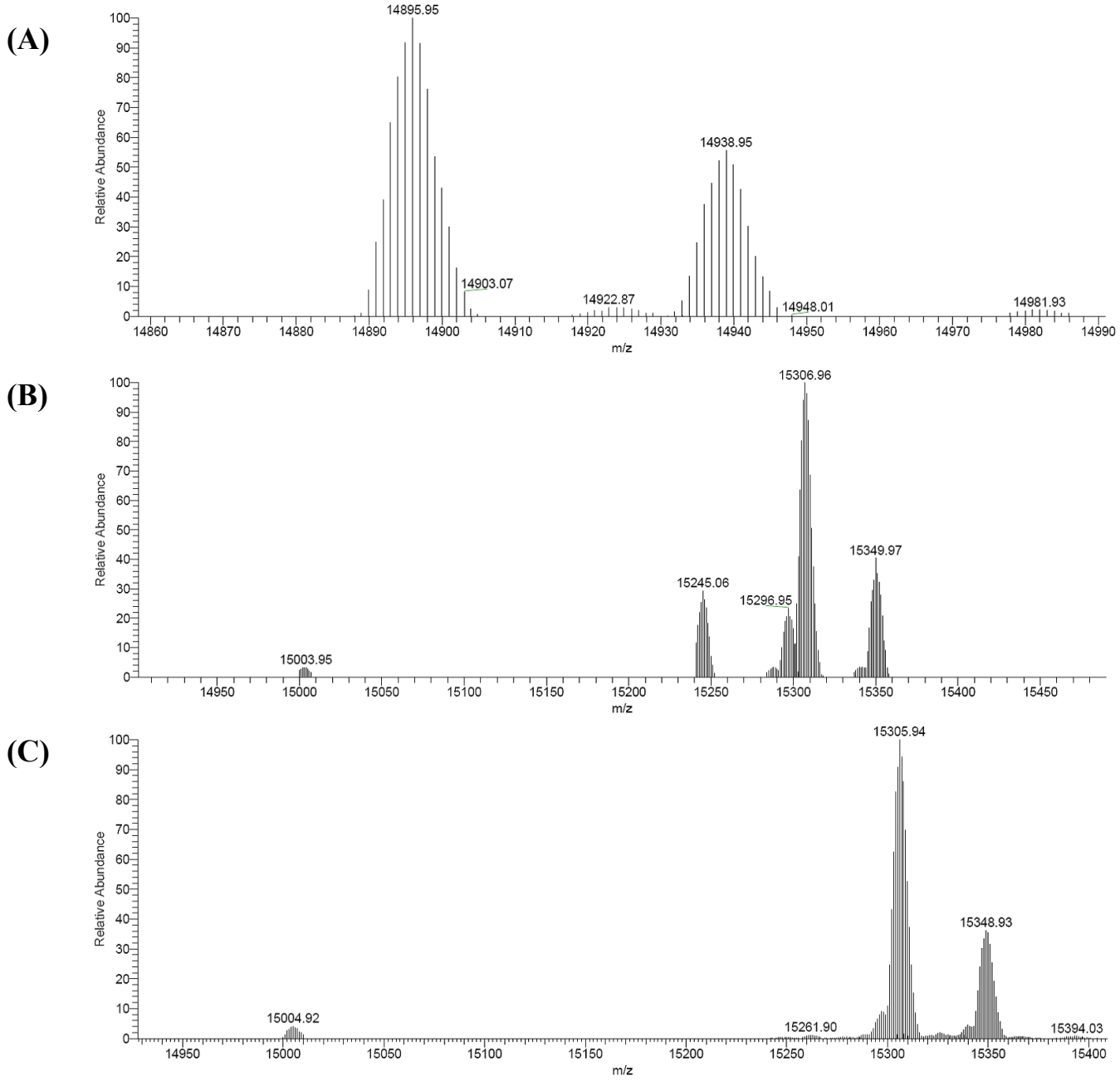

Figure 4. Analysis of K88C and its derivatives by an Orbitrap ESI-mass spectrometer. **(A)** K88C: the expected average mass of this species is 14,896.1 Daltons (Da); the +43 Da mass shift from the anticipated 14,895.95 Da peak to the 14,938.95 Da peak is consistent with lysine carbamylation, which is commonly observed if old or heated urea stocks have been used in protein purifications [47-49]. **(B)** K88C-EDTA: the expected average mass of this species is 15,245.5 Da. Peaks other than the anticipated one could result from a combination of lysine carbamylation and metal contamination, as EDTA is capable of binding many transition metals with a mass around 55 Da. **(C)** K88C-EDTA-Mn^{2+}: the expected average mass of this species is 15,297.4 Da. As with the K88C and K88C-EDTA species, the second major peak could be the result of lysine carbamylation.

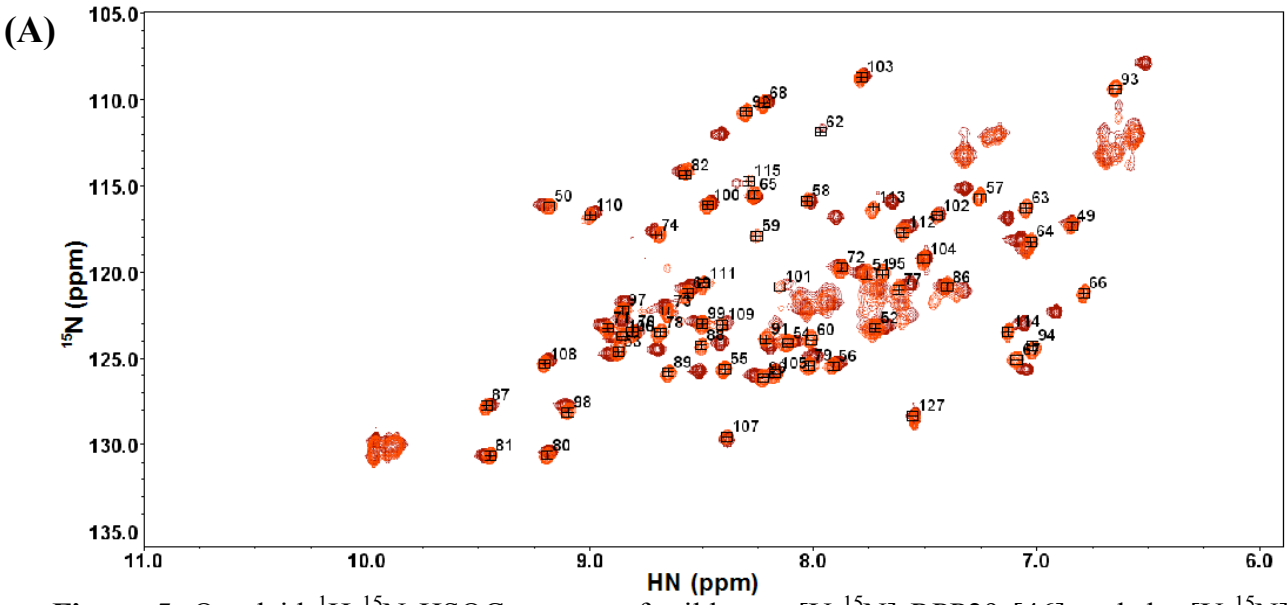

Figure 5. Overlaid ^{1}H-^{15}N HSQC spectra of wild type [U-^{15}N] RPP29 [46] and the [U-^{15}N]-C94A RPP29 mutant [Xu and Foster, unpublished]. **(A)** The wild type spectrum is red, while the spectrum for the C94A mutant is orange. Spectral assignments are for peaks in the spectrum of the C94A mutant.

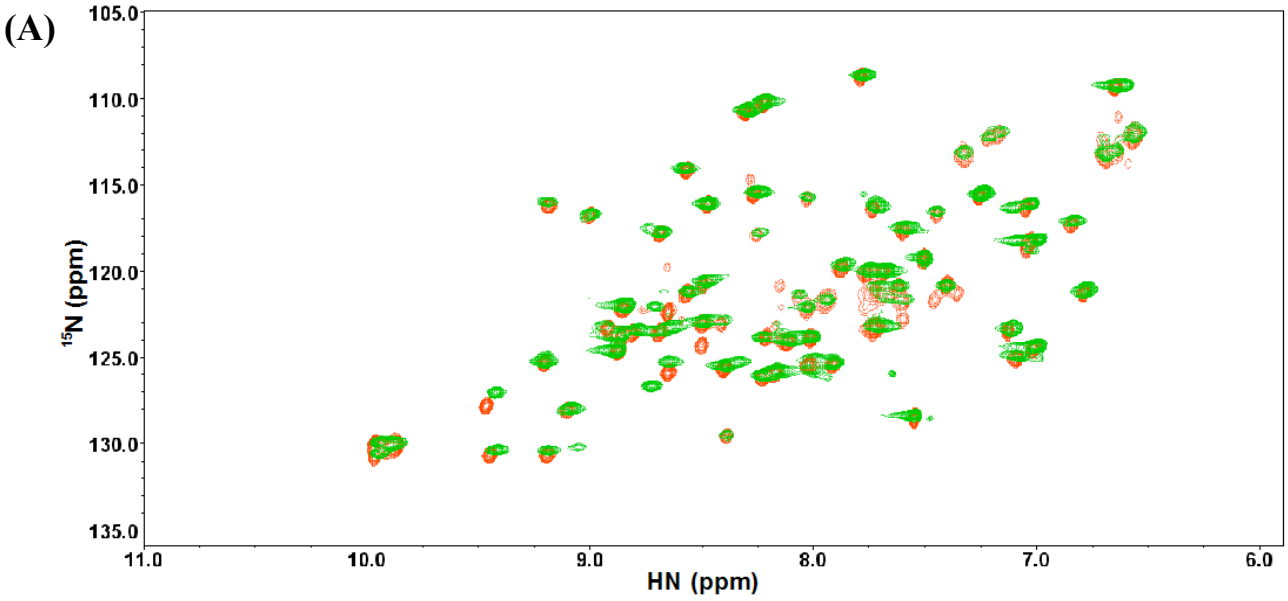

Figure 6. Overlaid ^{1}H-^{15}N HSQC spectra of the [U-^{15}N]-C94A RPP29 mutant [Xu and Foster, unpublished] and the [U-^{15}N]-K88C/C94A RPP29 mutant. **(A)** The spectrum of the C94A mutant is orange, while the spectrum of the K88C/C94A mutant is green.

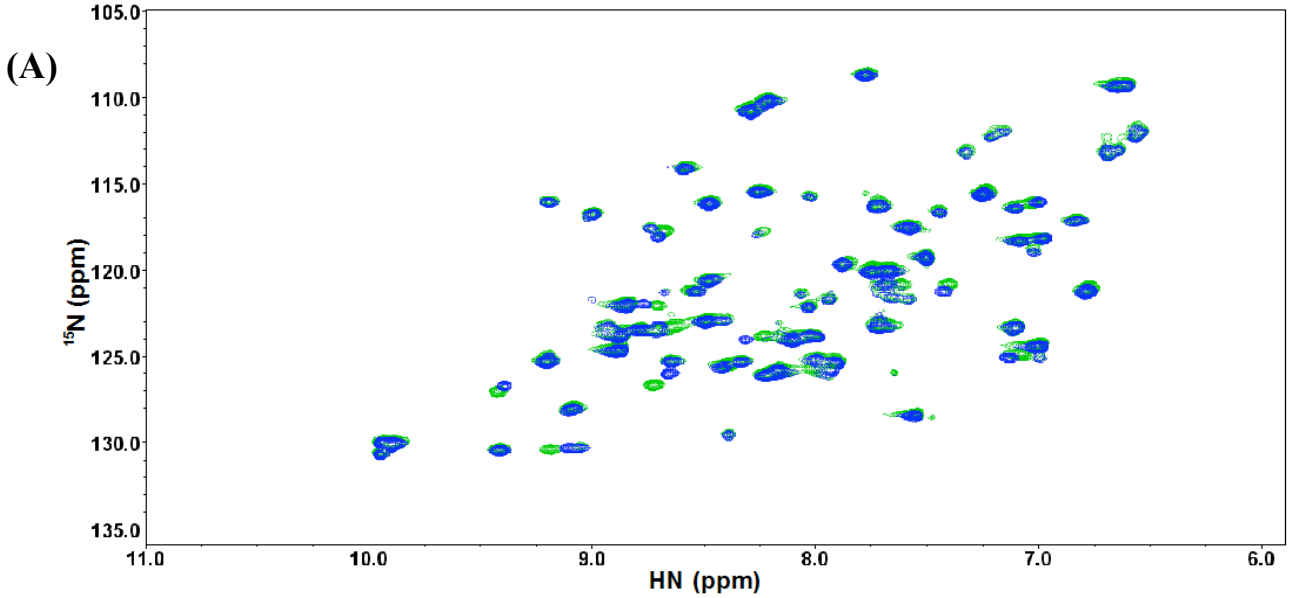

Figure 7. Overlaid ^{1}H-^{15}N HSQC spectra of the [U-^{15}N]-K88C/C94A RPP29 mutant and the [U-^{15}N]-K88C/C94A-EDTA species. **(A)** The spectrum of the [U-^{15}N]-K88C/C94A mutant is green, while the spectrum of the [U-^{15}N]-K88C/C94A-EDTA species is blue.

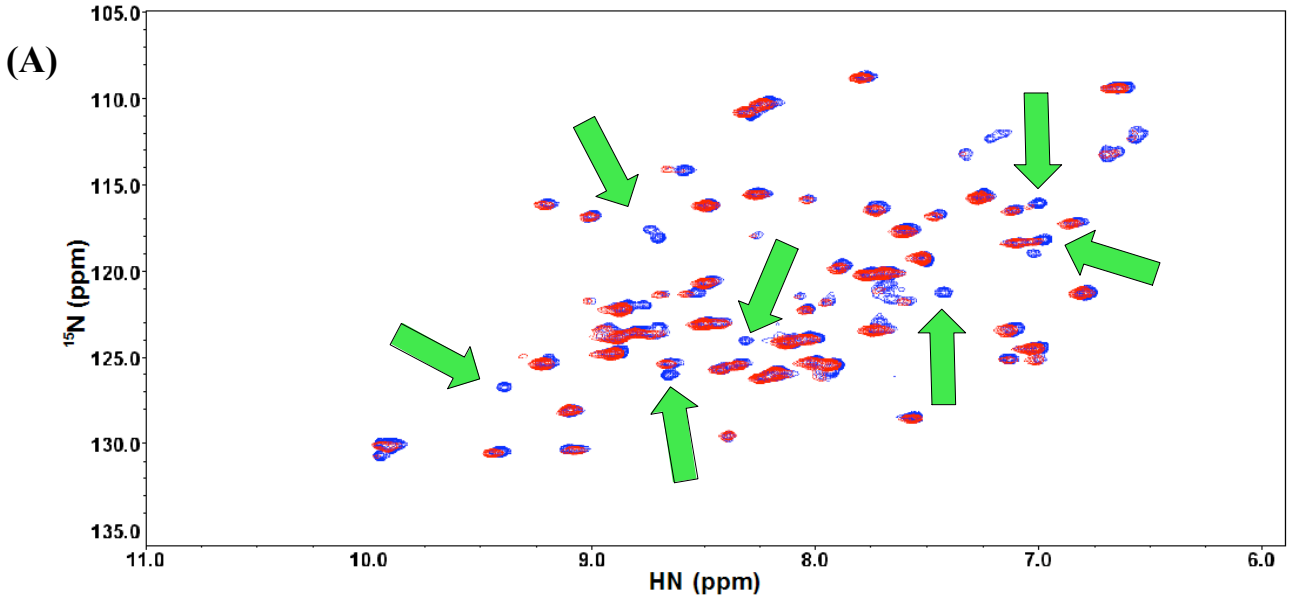

Figure 8. Overlaid ^{1}H-^{15}N HSQC spectra of the [U-^{15}N]-K88C/C94A-EDTA species and the [U-^{15}N]-K88C/C94A-EDTA-Mn^{2+} species. **(A)** The spectrum of the [U-^{15}N]-K88C/C94A-EDTA species is blue, while the spectrum of the [U-^{15}N]-K88C/C94A-EDTA-Mn^{2+} species is red. PRE is indicated by peaks in the pink spectrum that have partially or completely disappeared in the purple spectrum, as highlighted by the green arrows.

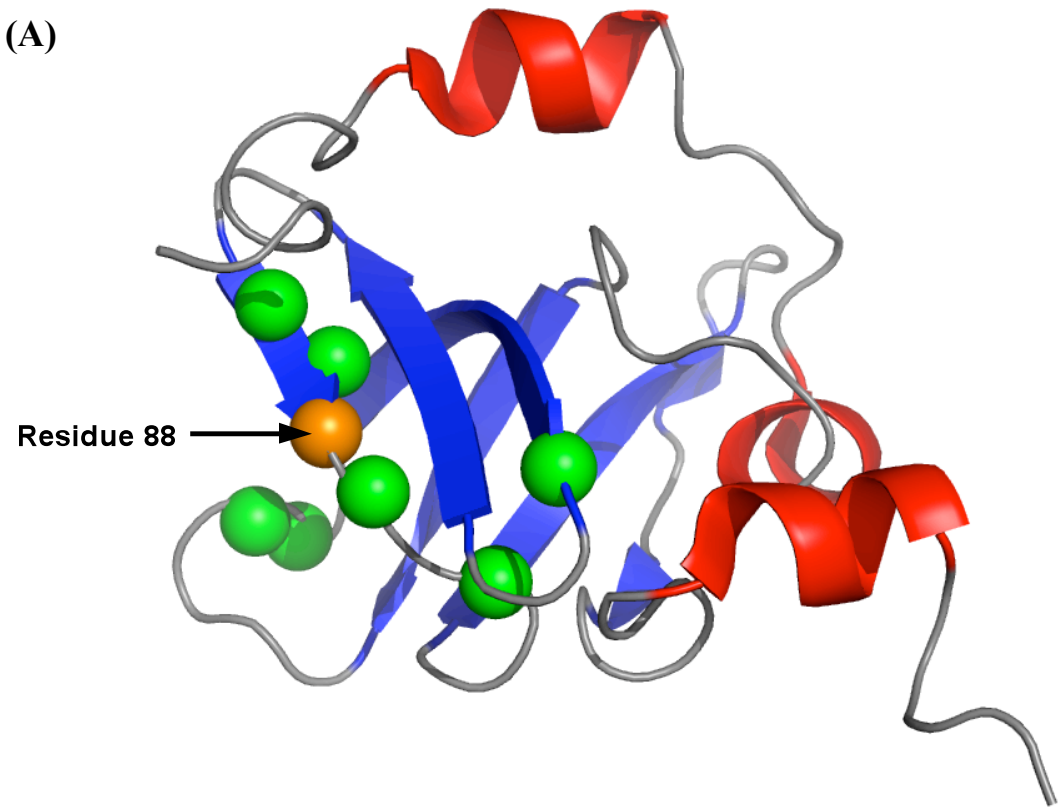

Figure 9. Mapping the effects of PRE to the structure of *Pfu* RPP29. **(A)** Green spheres indicate the protein residues that showed the largest response to the introduction of the paramagnetic Mn^{2+} probe: V64, Y63, T74, V86, W87, V89, and K91. Residue 88, the site of the attachment of the EDTA moiety, is indicated by the orange sphere.

(A)

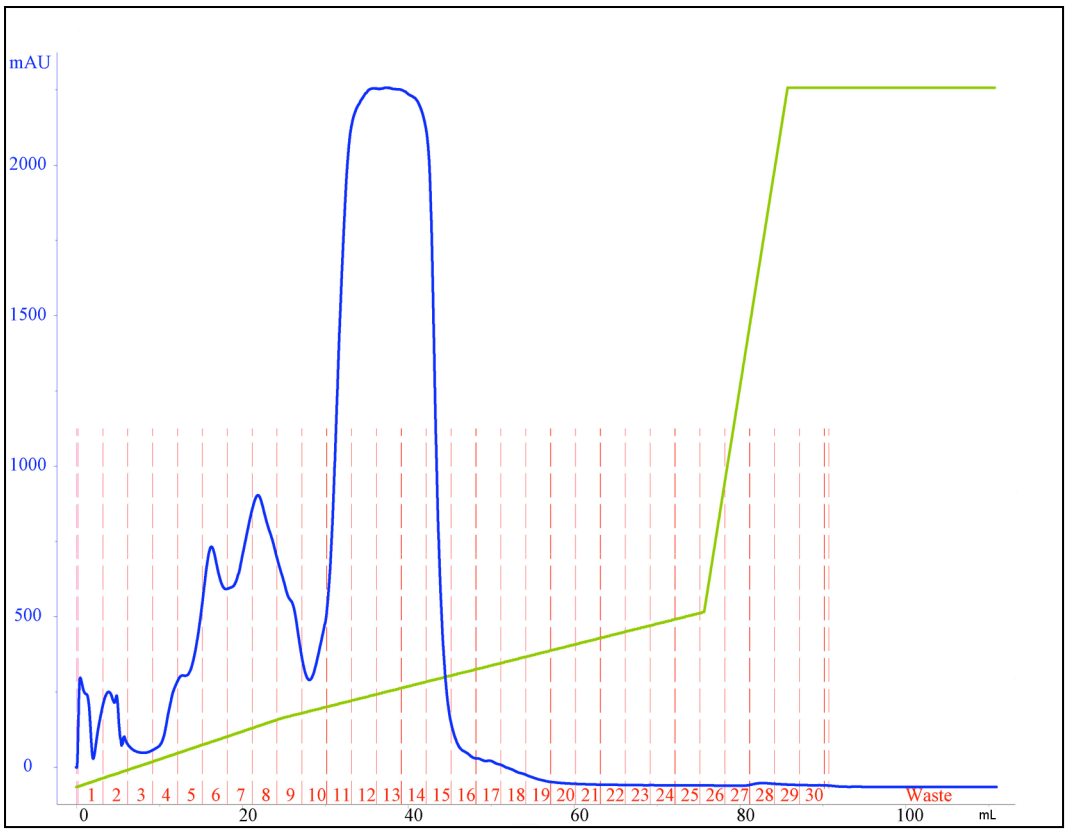

(B)

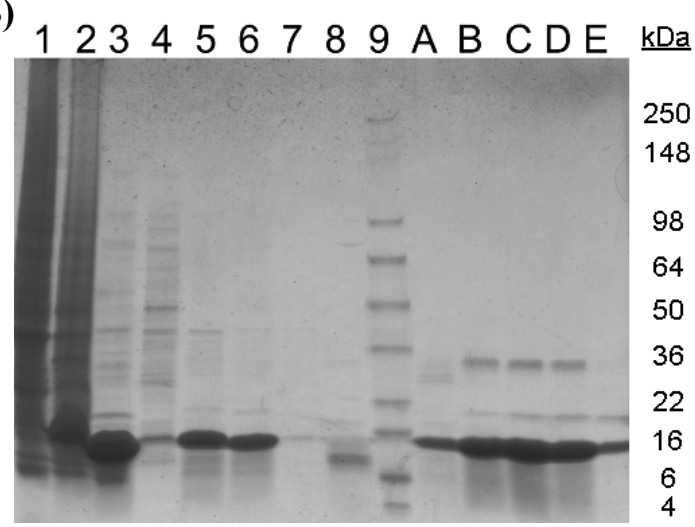

Figure 10. Purification of unlabeled K88C protein for RNA footprinting experiments.

(A) In this FPLC chromatogram, the green curve represents the volume percent of Buffer B that is in the column. About half of the protein has eluted by the time the [KCl] reaches 300 mM, which is around 14 % Buffer B. The blue curve represents the UV absorbance at 280 nm of the eluting material from the column, and the dashed red line segments delineate the different eluate fractions; fractions 12-14 contained the K88C protein.

(B) In this 4-20 % Tris-HCl SDS-PAGE gel (stained with Coomassie Brilliant Blue dye), lane one is K88C before induction, lane two is induced K88C, lane three is the pellet form the first centrifugation step, lane four is the soluble fraction from the first centrifugation step, lane five is the pellet from the second centrifugation step, lane six is the soluble fraction from the second centrifugation step, lane seven is the SP column flow-through, lane eight is fraction 8 (from the FPLC run), lane nine is the SeeBlue Plus2 Pre-Stained Standard protein ladder, and lanes A-E correspond to fractions 11-15, respectively. The data from the chromatogram and the gel suggest that relatively pure K88C was successfully purified.

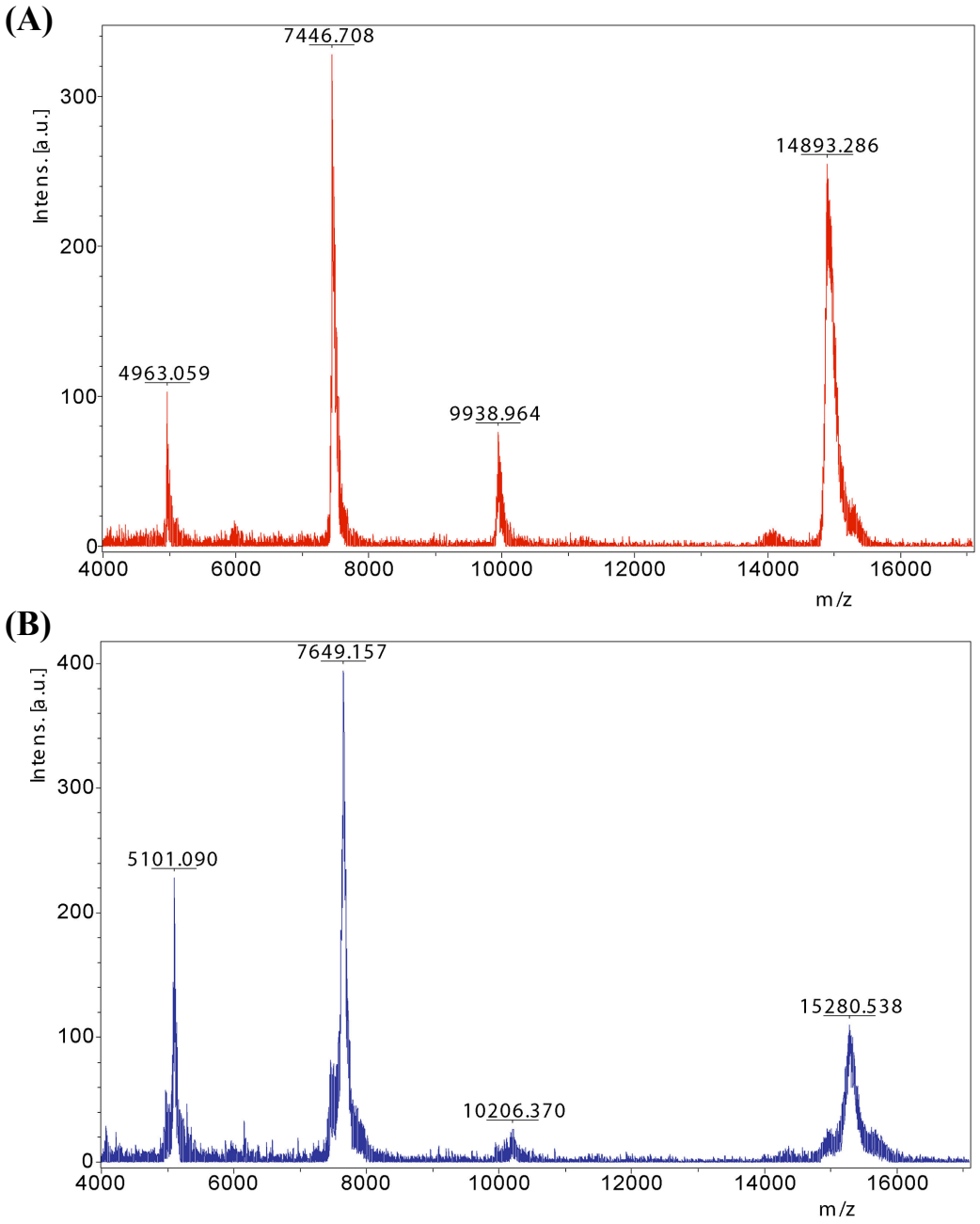

Figure 11. MALDI mass spectra confirm the EPD-Fe modification of the K88C protein. **(A)** K88C: in this mass spectrum, the expected mass/charge ratios (in Da/elementary charge) of the (z = +1), (z = +2), and (z = +3) states were 14,897.1, 7,749.05, and 4,966.36, respectively. Furthermore, the expected mass/charge ratio for the (z = +3) state of the protein dimer was 9,931.06. **(B)** K88C-EDTA-Fe: in this mass spectrum, the expected mass/charge ratios of the (z = +1), (z = +2), and (z = +3) states were 15,303.3, 7,652.2, and 5,101.8, respectively. Moreover, the expected mass/charge ratio for the (z = +3) state of the protein dimer was 10,202.5.

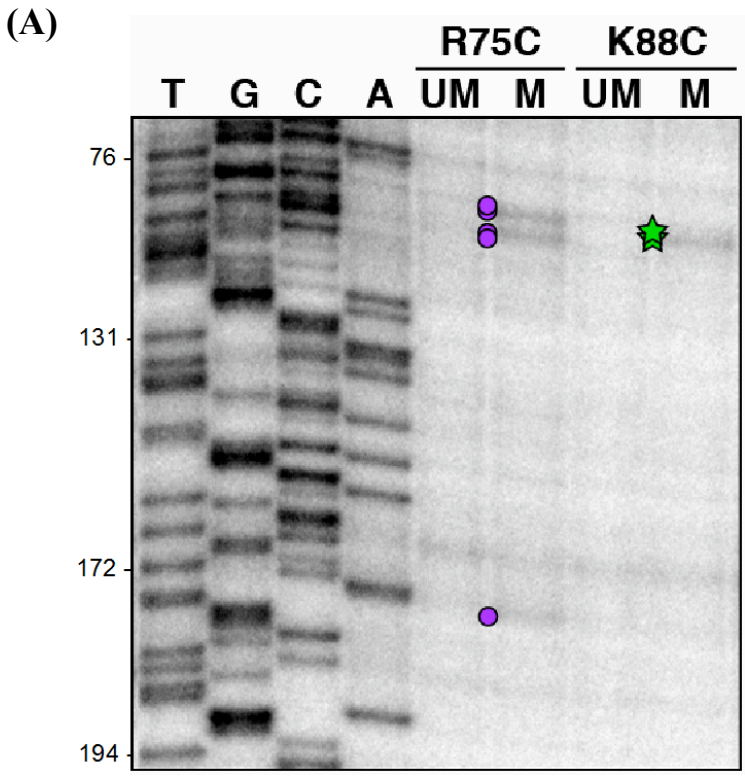

Figure 12. RNA footprinting products subjected to polyacrylamide gel electrophoresis and autoradiography. [Lai, Foster and Gopalan, unpublished]. **(A)** The first four lanes contain ^{32}P-labeled, dideoxynucleoside triphosphates (ddNTPs) of the indicated base (thymine, guanine, cytosine, and adenine, respectively) as well as unlabeled NTPs. These lengths report on the specific sites of the RNA cleavage, and cleavage sites for the R75C-EDTA-Fe and K88C-EDTA-Fe species are depicted by purple circles and green stars, respectively.

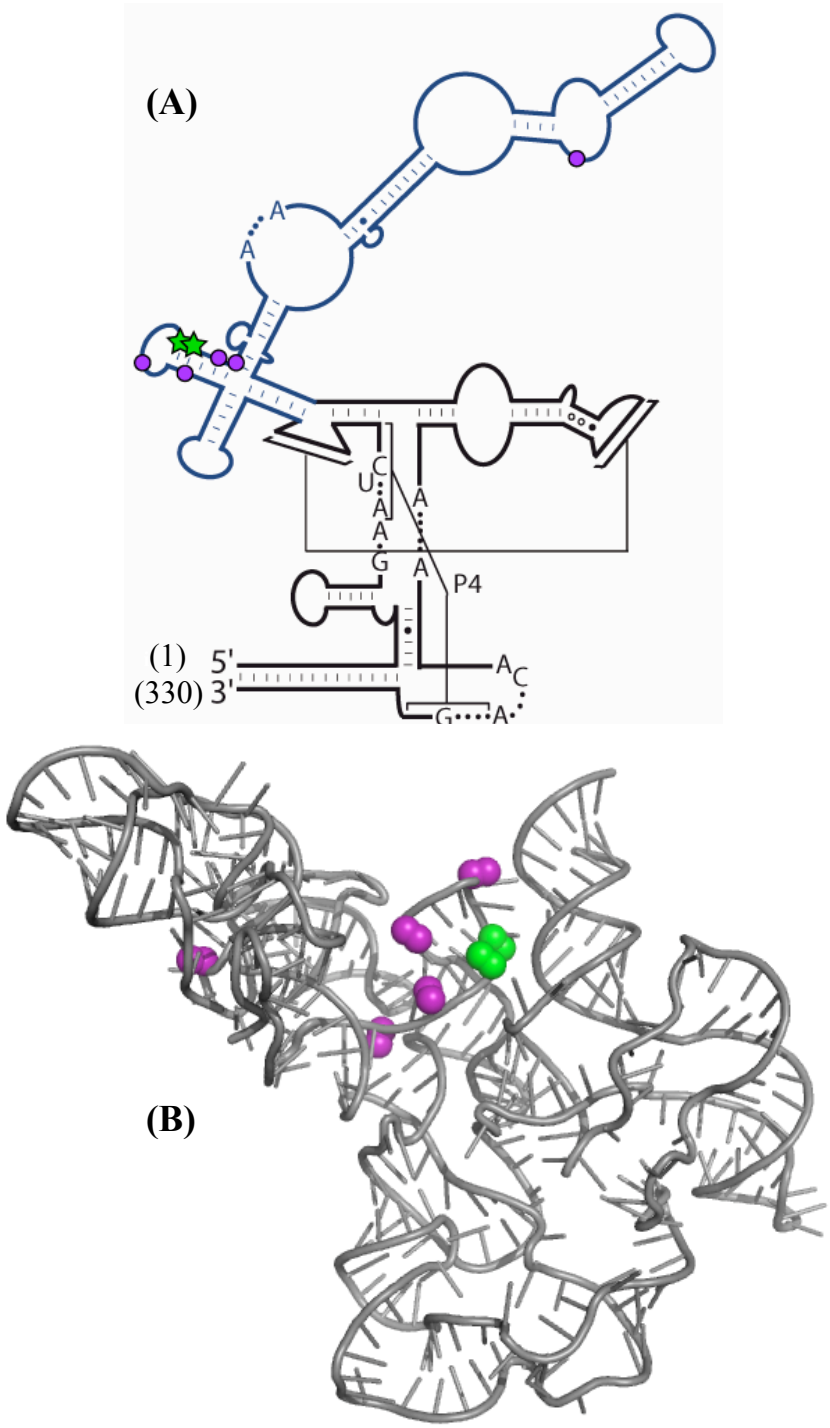

Figure 13. RNA footprinting cleavage sites mapped to the RPR structure. **(A)** In this two-dimensional representation of the *Pfu* RPR [Lai, Foster and Gopalan, unpublished], cleavage sites from R75C-EDTA-Fe and K88C-EDTA-Fe are represented by purple circles and green stars, respectively. **(B)** In this three-dimensional model of the *Pfu* RPR [Crowe and Foster, unpublished], hydroxyl-radical cleavage sites from R75C-EDTA-Fe and K88C-EDTA-Fe are represented by purple spheres and green spheres, respectively.